VOL 3, NO. 11: NOVEMBER 2026
AN OPEN ACCESS PEER-REVIEWED JOURNAL

*Frontline Professionals Journal* 3(11), 281-301, EISSN 1596-0501

***Original Research Article***

# ELECTROCHEMICAL STUDY OF MILD STEEL CORROSION IN 1 M HCL: COMPARATIVE INHIBITION PERFORMANCE OF QUERCETIN-RICH RED ONION SKIN AND CURCUMIN-RICH TURMERIC EXTRACTS.

**Authors: Samson Uchenna Eze[1]*, Jude Ebere Kanu[1,2], Abosede Olubunmi James[2], Ozioma Achugasim[2], Uche John Chukwu[2], Onyewuchi Akaranta[2], Abuchi Elebo[3]**

[1]Department of Chemistry, Federal College of Education (Technical), Omoku, Rivers State, Nigeria
[2]Department of Chemistry, University of Port Harcourt, Nigeria
[3]Department of Industrial Chemistry, Faculty of Sciences. Federal University of Applied Sciences Kachia, Kaduna State

Corresponding Author: Samson Uchenna Eze
Email: ezesamson@fcetomoku.edu.ng
*Tel: +2348135791204

***Author's contributions***

*This study was a collaborative effort of the authors. The authors reviewed and approved the final version of the manuscript for publication.*

***Article Information***

***DOI: https://doi.org/10.60787/fpj.vol3no11.148***

*EISSN 1596-0501E*

*This work is licensed under a* Creative Commons Attribution-Non-Commercial-ShareAlike 4.0 International License

**CITATION:** Eze, U. S., Kanu, E. J., James, O. A., Achugasim, O., Chukwu, U. J., Akaranta, O., & Elebo, A. (2026). Electrochemical study of mild steel corrosion in 1 M HCl: Comparative inhibition performance of quercetin-rich red onion skin and curcumin-rich turmeric extracts. *Frontline Professionals Journal* 3(11), 281-301

## ABSTRACT

This study comparatively investigated the corrosion inhibition performance of quercetin-rich red onion skin extract (ROSE) and curcumin-rich turmeric extract (TE) on mild steel in 1 M hydrochloric acid (HCl). The plant materials were collected, authenticated, dried, pulverised and separately extracted using absolute ethanol through cold maceration for 48 h. The resulting extracts were subjected to qualitative and quantitative phytochemical analyses, melting point determination, solubility testing, Fourier-transform infrared (FTIR) spectroscopy, ultraviolet–visible (UV–Vis) spectroscopy and scanning electron microscopy coupled with energy-dispersive X-ray spectroscopy (SEM–EDX). Their corrosion inhibition properties were evaluated at concentrations of 0.2–0.5 g/L using open-circuit potential (OCP), potentiodynamic polarisation (PDP) and electrochemical impedance spectroscopy (EIS). Phytochemical analysis identified quercetin (34.4772 µg/mL) and curcumin (40.2159 µg/mL) as the predominant quantified constituents of ROSE and TE, respectively. FTIR indicated hydroxyl, carbonyl and other oxygen-containing functional groups. Both extracts exhibited mixed-type inhibition behaviour. ROSE achieved maximum PDP and EIS inhibition efficiencies of 98.24% and 98.56%, respectively, at 0.4 g/L, while TE recorded maximum efficiencies of 97.30% and 98.04%, respectively, at 0.4 and 0.5 g/L. Overall, ROSE demonstrated stronger inhibition performance at 0.4 g/L, establishing both extracts as promising plant-derived corrosion inhibitors for mild steel in 1 M HCl.

Keywords: Mild steel corrosion; Green corrosion inhibitors; Red onion skin extract; Turmeric extract; Quercetin; Curcumin.

## INTRODUCTION

Mild steel is widely employed in engineering, construction, manufacturing, and petroleum industries because of its affordability, mechanical strength, and ease of fabrication. However, its susceptibility to corrosion, particularly in acidic environments, limits its durability and service performance. Hydrochloric acid is frequently used in industrial operations such as acid pickling, descaling, and cleaning, where prolonged exposure can accelerate metal dissolution and compromise material integrity (Emmanuel, 2024; Medupin *et al.,* 2023). The corrosion of mild steel in acidic environments involves electrochemical reactions, principally anodic iron dissolution and cathodic hydrogen evolution. Consequently, effective corrosion control is essential to minimise material degradation, maintenance costs, and operational failures (Shwetha *et al.,* 2024). The application of corrosion inhibitors is an established approach to reducing metal deterioration in aggressive environments. However, concerns regarding the toxicity, environmental persistence, and disposal of some conventional synthetic inhibitors have encouraged the investigation of environmentally friendly alternatives. Plant-derived extracts have attracted considerable interest because they contain naturally occurring organic compounds with heteroatoms, aromatic rings, conjugated systems, and functional groups capable of interacting with metallic surfaces. Through adsorption, these constituents can establish protective interfacial layers that restrict the electrochemical reactions responsible for corrosion (Nikolaychuk *et al.,* 2023; Hjouji *et al.,* 2023). Several investigations have demonstrated the effectiveness of plant extracts in protecting mild steel in hydrochloric acid through electrochemical and surface-characterisation techniques (Sowmyashree *et al.,* 2023; Yıldız *et al.,* 2024).

Red onion skin (*Allium cepa L.*) and turmeric (*Curcuma longa L.*) represent promising botanical sources of corrosion-inhibiting compounds. Red onion skin contains quercetin, a polyphenolic flavonoid characterized by hydroxyl groups, carbonyl functionality, and conjugated aromatic structures. Similarly, turmeric contains curcumin, a polyphenolic compound with phenolic hydroxyl groups, methoxy substituents, and a conjugated β-diketone system. These structural characteristics provide potential adsorption centres for interaction with metallic surfaces. Previous investigations have established the corrosion-inhibiting potential of naturally occurring polyphenolic and plant-derived compounds, including flavonoid-rich extracts (Teng *et al.,* 2021; Kumar, H. *et al.,* 2022; Kumar, M. *et al.,* 2022; Doumane *et al.,* 2024). Despite the growing interest in plant-based corrosion inhibitors, a comparative electrochemical investigation of quercetin-rich red onion skin and curcumin-rich turmeric extracts under identical acidic conditions provides an important basis for evaluating their relative protective performance. In particular, relating their phytochemical composition and spectroscopic characteristics to their electrochemical responses provides a broader understanding of their inhibition behaviour. Therefore, this study comparatively investigates the corrosion inhibition performance of ethanolic red onion skin extract (ROSE) and turmeric extract (TE) on mild steel in 1 M HCl. The extracts were subjected to qualitative and quantitative phytochemical analysis, melting point determination, solubility testing, Fourier-transform infrared (FTIR) spectroscopy, UV–visible spectroscopy, and scanning electron microscopy coupled with energy-dispersive X-ray spectroscopy (SEM–EDX). Their corrosion inhibition performance was evaluated at concentrations of 0.2–0.5 g/L using open-circuit potential (OCP), potentiodynamic polarisation (PDP), and electrochemical impedance spectroscopy (EIS). The study further establishes a comparative assessment of their inhibition efficiencies using PDP and EIS measurements, with particular attention to the contributions of quercetin-rich and curcumin-rich constituents to their corrosion-protection behaviour.

## MATERIALS AND METHODS

Materials**:** Fresh red onion skins (*Allium cepa* L.) and turmeric rhizomes (*Curcuma longa* L.) were collected from Omoku, Ogba/Egbema/Ndoni Local Government Area (ONELGA), Rivers State, Nigeria. The plant materials were taxonomically identified and authenticated at the Department of Plant Science, University of Port Harcourt, Rivers State, Nigeria. Analytical-grade hydrochloric acid (HCl), absolute ethanol, distilled water, acetone, sodium hydroxide, ferric chloride, Wagner's reagent, Mayer's reagent, Dragendorff's reagent, concentrated sulphuric acid, chloroform, and other chemicals required for phytochemical screening were obtained from standard chemical suppliers and used without further purification. Mild steel coupons used for the corrosion experiments were obtained from ACFOR Laboratory, Rivers State, Nigeria. All chemicals and reagents were used as received.

Mild Steel Preparation**:** The mild steel sheets were mechanically cut into rectangular coupons of uniform dimensions and perforated near one edge to facilitate suspension during immersion experiments. The exposed surfaces were successively polished using silicon carbide abrasive papers of different grit sizes to obtain a smooth surface finish, rinsed thoroughly with distilled water, degreased with acetone, washed again with distilled water, and air-dried. Each coupon was weighed using a digital analytical balance with a precision of ±0.001 g, and its initial mass was recorded where required. Freshly prepared 1 M hydrochloric acid (HCl) served as the corrosive medium, while the ethanolic extracts of red onion skin (*Allium cepa L.*) and turmeric (*Curcuma longa L.*) were separately introduced at the required concentrations to evaluate their corrosion inhibition performance. The electrochemical behaviour of mild steel in the uninhibited and inhibited solutions was investigated using open-circuit potential (OCP), potentiodynamic polarisation (PDP), and electrochemical impedance spectroscopy (EIS).

Preparation of Red Onion Skin (*Allium cepa L.*) and Turmeric (*Curcuma longa L.*) Extracts**:** The red onion skins and turmeric rhizomes were separately washed under running tap water, rinsed with distilled water, and air-dried under laboratory conditions until completely dry. The dried samples were independently ground into fine powders using an electric laboratory grinder and stored in airtight containers until extraction. For each plant material, 100 g of the powdered sample was transferred into a suitable container and extracted with 600 mL of absolute ethanol by cold maceration for 48 h, with intermittent shaking to enhance contact between the plant material and extraction solvent. The resulting mixtures were filtered using Whatman No. 1 filter paper, and the filtrates were concentrated using a rotary evaporator, followed by gentle evaporation on a water bath to obtain the respective crude ethanolic extracts. The concentrated extracts were separately transferred into airtight containers and stored at 4°C until required. Stock inhibitor solutions were prepared by dissolving appropriate quantities of each crude extract separately in 1 M HCl to obtain the desired working concentrations for subsequent electrochemical investigations. Similar extraction and evaluation approaches have been reported in studies involving plant-derived corrosion inhibitors (Miralrio & Espinoza Vázquez, 2020). Phytochemical Analysis: Phytochemical analysis was conducted to identify and quantify bioactive constituents in the ethanolic extracts of red onion skin (*Allium cepa L.*) and turmeric (*Curcuma longa L.*). Extract cleanup involved activated Florisil and anhydrous sodium sulphate, followed by n-hexane elution and rotary evaporation. The prepared samples were subjected to GC-FID analysis using a BUCK gas chromatograph, with compound concentrations estimated from analyte and internal-standard peak-area relationships. The identified phytochemicals were considered relevant to corrosion inhibition because their oxygen-containing functional groups, heteroatoms and conjugated π-electron systems may facilitate adsorption and donor–acceptor interactions with mild steel, potentially promoting protective films that limit contact with the acidic medium (Chidiebere *et al.,* 2024; Miralrio & Espinoza Vázquez, 2020).

Characterization of Red Onion Skin and Turmeric Extracts: The red onion skin and turmeric extracts were characterized using UV–visible, Fourier transform infrared (FTIR), and scanning electron microscopy (SEM) techniques. For UV–visible analysis, approximately 0.1 g of each extract was separately dissolved in 10 mL of ethanol, filtered, and scanned from 190–800 nm using an Apel PD30000UV spectrophotometer equipped with a 10-mm quartz cell. FTIR analysis was performed using a Buck 530 IR spectrophotometer, with approximately 0.1 g of each extract mixed with 0.5 g of potassium bromide (KBr) and 1 mL of Nujol. The spectra were recorded within 600–4000 $cm^{-1}$ to identify the functional groups responsible for possible interactions with the mild steel surface. SEM analysis was conducted using a Phenom ProX microscope to examine the morphological characteristics of the extracts. Approximately 0.1 g of each sample was mounted on double-sided adhesive tape, coated with 5 nm of gold using a Quorum Q150R sputter coater, and examined at different magnifications.

Melting Point Determination and Solubility Test of Red Onion Skin and Turmeric Extracts: The melting points of the red onion skin and turmeric extracts were determined by separately introducing approximately 0.5 g of each extract into suitable capillary tubes and heating gradually in a calibrated Gallenkamp melting point apparatus. The temperatures at which melting commenced and was completed were recorded. The solubility characteristics of the extracts were also investigated by separately transferring approximately 0.1 g of each into clean, labelled test tubes, followed by the gradual addition of selected solvents. The mixtures were shaken thoroughly at room temperature, and their dissolution

behaviour was recorded as soluble, slightly soluble, or insoluble. Where necessary, gentle warming in a water bath was applied, and any changes in solubility were observed and recorded for comparison.

**Corrosion Studies**

The corrosion inhibition performance of red onion skin extract (ROSE) and turmeric extract (TE) was evaluated using electrochemical techniques, namely open-circuit potential (OCP), potentiodynamic polarisation (PDP) and electrochemical impedance spectroscopy (EIS). These techniques provided complementary information on the electrochemical behaviour of mild steel, corrosion kinetics and changes occurring at the metal–solution interface in 1 M HCl in the presence of the extracts. The results were used to compare the inhibition efficiencies of ROSE and TE and assess their protective effects and possible corrosion-inhibition mechanisms.

Electrochemical Measurements**:** Electrochemical investigations were conducted in 1 M HCl corrosive electrolyte, with and without different concentrations of ROSE and TE, at room temperature. Measurements were performed using a Metrohm Autolab potentiostat (PGSTAT204) interfaced with NOVA 2.14 software. A conventional three-electrode electrochemical cell was employed, consisting of mild steel with an exposed surface area of 1 $cm^2$ as the working electrode, a platinum wire as the counter electrode and a silver/silver chloride (Ag/AgCl) electrode as the reference electrode. All reported electrode potentials were measured against the Ag/AgCl reference electrode. Before the electrochemical measurements, the working electrode was immersed in the test solution, and the open-circuit potential (OCP) was monitored for 1800 s (30 min) to allow the system to attain a stable potential. The stabilised OCP was taken as the corrosion potential (Ecorr) of the metal in the test environment. Potentiodynamic polarisation (PDP) measurements were subsequently performed at a scan rate of 0.2 mV $s^{-1}$ over the selected potential range relative to OCP. The corrosion potential (Ecorr), corrosion current density (Icorr), anodic Tafel slope (βa), cathodic Tafel slope (βc) and inhibition efficiency were obtained from the polarisation curves using Tafel extrapolation. The PDP inhibition efficiency was calculated using Equation (1) (Ferreira *et al.,* 2004):

$$IE_{PDP}(\%) = \left(1 - \frac{\mathrm{i_{corr}}}{\mathrm{i^0_{corr}}}\right) \times 100 \qquad 1$$

Where $\mathbf{i}^0_{\mathrm{corr}}$ and $\mathrm{i_{corr}}$ are the corrosion current densities in the absence and presence red onion skin and turmeric extracts, respectively.

Electrochemical impedance spectroscopy (EIS) measurements were performed at the stabilised OCP using a sinusoidal perturbation signal with an amplitude of 10 mV over a frequency range of 100 kHz to 10 mHz. The impedance spectra were analysed using Nyquist and Bode plots. The fitted parameters reported in Tables 3.6 and 3.8 include solution resistance (Rs), pore resistance (Rpo), charge-transfer resistance (Rct) and the constant-phase-element parameters (Q1, n1, Q2 and n2). The EIS data were fitted using ZSimpWin version 3.2, with an equivalent circuit selected to represent the metal–electrolyte system. The EIS inhibition efficiency was calculated from the charge-transfer resistance using Equation (2) (Umoren *et al.,* 2009):

$$IE_{\boldsymbol{EIS}}(\%) = \left(1 - \frac{\mathrm{R^0_{ct}}}{\mathrm{R_{ct}}}\right) \times 100 \qquad 2$$

Where $\mathrm{R^0_{ct}}$and $\mathrm{R_{ct}}$ represent the charge transfer resistance values in the absence and presence of the inhibitor, respectively. An increase in Rct indicates greater resistance to interfacial charge transfer, suggesting improved protection of the mild steel surface. Changes in the constant-phase-element parameters indicate modifications in the interfacial capacitive response following the addition of the extracts. The PDP data were analysed using EC-Lab software, while the electrochemical data and plots were processed using OriginPro 2016.

**RESULTS AND DISCUSSION**

Phytochemical Composition of Red Onion Skin and Turmeric Extracts: The quantitative phytochemical composition of the red onion skin extract (ROSE) and turmeric extract (TE) is presented in Tables 3.1 and 3.2, respectively. The results indicate that quercetin was the predominant quantified constituent of ROSE, with a concentration of 34.4772 µg/mL out of a total quantified phytochemical concentration of 57.6338 µg/mL. This represents approximately 59.82% of the total quantified constituents, demonstrating the quercetin-rich character of the red onion skin extract. Other identified constituents included tannins (4.6825 µg/mL), terpenoids (4.0523 µg/mL), flavones (3.8463 µg/mL), sapogenin (3.7252 µg/mL), and kaempferol (3.4121 µg/mL). The remaining constituents were present at lower concentrations.

**Table 3.1:** Phytochemical Composition of Red Onion Skin Extract (ROSE)

| S/N | Phytochemical components | Concentration (µg/mL) |
|---|---|---|
| 1 | Alkaloids | 2.2955 |
| 2 | Sapogenin | 3.7252 |
| 3 | Cyanogenic glycoside | 1.0926 |
| 4 | Quercetin | 34.4772 |
| 5 | Tannin | 4.6825 |
| 6 | Flavones | 3.8463 |
| 7 | Kaempferol | 3.4121 |
| 8 | Terpenoids | 4.0523 |
| 9 | Epicatechin | 1.0668 |
| 10 | Phenol | 1.0132 |
| | **Total** | **57.6338** |

Similarly, curcumin was the predominant quantified constituent of TE, with a concentration of 40.2159 µg/mL from a total quantified concentration of 65.8602 µg/mL, accounting for approximately 61.04% of the total quantified phytochemicals. Other constituents included flavan-1-one (4.7121 µg/mL), sapogenin (3.7653 µg/mL), phytate (3.0720 µg/mL), tannins (2.7625 µg/mL), and cyanogenic glycosides (2.4604 µg/mL). The remaining components occurred at comparatively lower concentrations.

**Table 3.2:** Phytochemical Composition of Turmeric Extract (TE)

| S/N | Phytochemical components | Concentration (µg/mL) |
|---|---|---|
| 1 | Alkaloids | 2.1119 |
| 2 | Steroids | 1.9519 |
| 3 | Phytate | 3.0720 |
| 4 | Cyanogenic glycoside | 2.4604 |
| 5 | Flavan-1-one | 4.7121 |
| 6 | Tannin | 2.7625 |
| 7 | Oxalate | 0.9652 |
| 8 | Sapogenin | 3.7653 |
| 9 | Naringenin | 0.9919 |
| 10 | Curcumin | 40.2159 |
| 11 | Terpenoids | 2.0691 |
| | **Total** | **65.8602** |

The predominance of quercetin and curcumin is particularly relevant to the intended corrosion-inhibition application. Quercetin contains several phenolic hydroxyl groups, a conjugated carbonyl group, and aromatic rings, providing oxygen-containing sites and π-electron systems that may participate in interactions with the mild steel surface. Curcumin also contains phenolic hydroxyl groups, methoxy substituents, aromatic rings, and a conjugated β-diketone system. These structural features provide potential adsorption centres through which the organic constituents may interact with the metal surface in an acidic environment (Dehghani *et al.,* 2020; Miralrio & Espinoza Vázquez, 2020;

Wei *et al.,* 2020). The phytochemical composition therefore establishes the presence of substantial quantities of the two principal constituents investigated in this study.

Physicochemical Properties of the Extracts: The melting temperature ranges of the extracts are presented in Table 3.3. ROSE exhibited a melting range of 78–102.40 °C, while TE melted within the range of 89–107.50 °C. The broad melting intervals indicate that the extracts contain mixtures of several organic constituents rather than single, highly purified substances. Consequently, the recorded temperatures represent the melting behaviour of the crude extracts.

**Table 3.3:** Melting point range of the Red Onion Skin Extract (ROSE) and Turmeric Extract (TE)

| S/N | Sample | Melting temperature ($^0$C) |
|---|---|---|
| 1 | ROSE | 78 - 102.40 |
| 2 | TE | 89 - 107.50 |

The solubility behaviour of the extracts in different solvents is presented in Table 3.4. Both extracts were soluble in ethyl acetate, dichloromethane, n-hexane, ethanol, chloroform, toluene, and dimethyl sulfoxide (DMSO), but insoluble in water. This behaviour indicates that the extracted constituents exhibit appreciable affinity for the organic solvents examined. Their insolubility in water is also relevant to their formulation and dispersion in aqueous corrosive media. Since the corrosion experiments were conducted in 1 M HCl, the actual dissolution and stability of each extract in the prepared inhibitor solutions remain important considerations.

**Table 3.4:** Solubility Behaviour of Red Onion Skin Extract (ROSE) and Turmeric Extract (TE)

| **S/N** | **Solvent** | **TE** | **ROSE** |
|---|---|---|---|
| 1 | Ethyl acetate | Soluble | Soluble |
| 2 | Dichloromethane | Soluble | Soluble |
| 3 | *n*-Hexane | Soluble | Soluble |
| 4 | Ethanol | Soluble | Soluble |
| 5 | Chloroform | Soluble | Soluble |
| 6 | Toluene | Soluble | Soluble |
| 7 | Dimethyl sulfoxide (DMSO) | Soluble | Soluble |
| 8 | Water | Insoluble | Insoluble |

Spectroscopic Characterization of the Extracts: Fourier-transform infrared spectroscopy (FTIR) was used to identify the principal functional groups present in the extracts. The FTIR spectra of ROSE and TE are presented in Figure 3.1. The ROSE spectrum exhibited absorption bands at approximately 3542.60 and 3239.52 $cm^{-1}$, which are attributable to O–H stretching vibrations associated with hydroxyl-containing constituents. The band at 3120.70 $cm^{-1}$ may be assigned to aromatic C–H stretching, while the absorption at 2901.12 $cm^{-1}$ is associated with aliphatic C–H stretching. The band at 1411.90 $cm^{-1}$ may be attributed to aromatic skeletal vibrations and O–H bending, while the absorption at 1284.82 $cm^{-1}$ is associated with C–O stretching vibrations. These absorption bands indicate the presence of hydroxyl-containing and aromatic constituents in ROSE. The oxygen-containing functional groups are important because they provide potential interaction sites for adsorption onto the mild steel surface (Dehghani *et al.,* 2020). For TE, the absorption bands observed at approximately 3357.86, 3200.96, and 3146.89 $cm^{-1}$ are associated with O–H stretching and overlapping hydrogen-bonded hydroxyl vibrations. The bands at 2962.15 and 2861.01 $cm^{-1}$ are attributable to aliphatic C–H stretching vibrations. An absorption band at 1614.31 $cm^{-1}$ may be assigned to conjugated carbonyl and aromatic C=C vibrations, while the band at 1544.81 $cm^{-1}$ is associated with aromatic skeletal vibrations. The absorptions at 1357.99 and 1265.08 $cm^{-1}$ are attributable to C–O-related vibrations and phenolic/enolic functional groups. The presence of these functional groups indicates that TE contains oxygen-bearing organic constituents with conjugated aromatic structures. In particular, the hydroxyl, carbonyl, and C–O-containing groups provide possible

adsorption centres, while the conjugated π-electron system may contribute to interactions between the extract constituents and the metal surface (Van Nong *et al.,* 2016; Boscariol *et al.,* 2022).

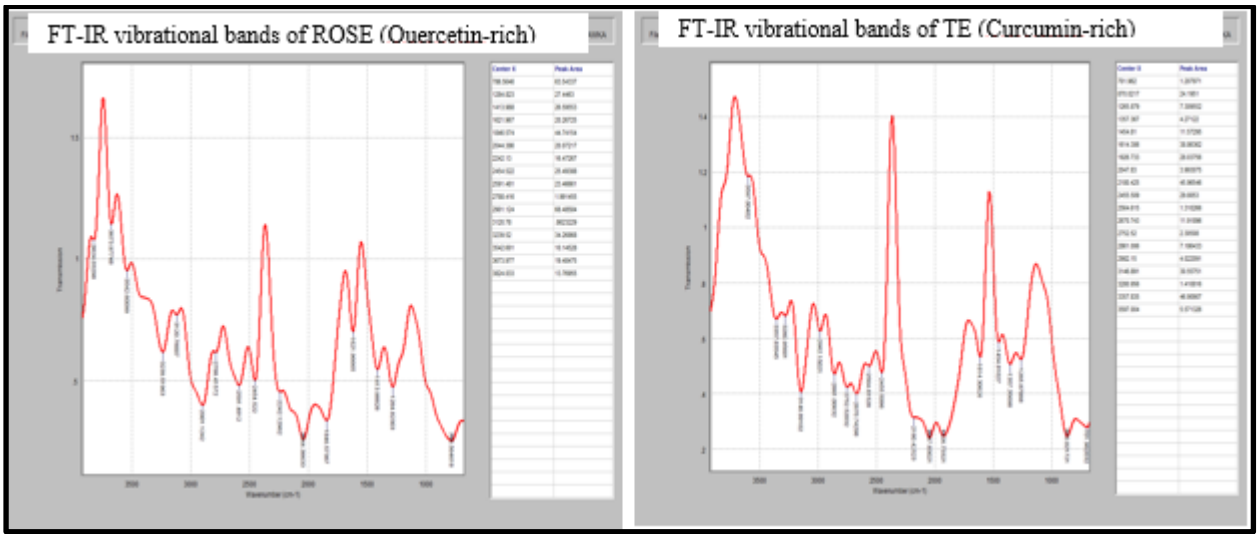



***Fig. 3.1*** *FT-IR vibrational bands of ROSE and TE.*

The UV–Visible absorption spectra of ROSE and TE are presented in Figure 3.2. The ROSE spectrum exhibited prominent absorption maxima at approximately 450 and 730 nm, with absorbance values of 1.821 and 1.882, respectively. The absorption in the visible region indicates the presence of light-absorbing chromophoric constituents within the extract. These absorptions may arise from electronic transitions involving conjugated structures and other coloured constituents present in the crude extract.

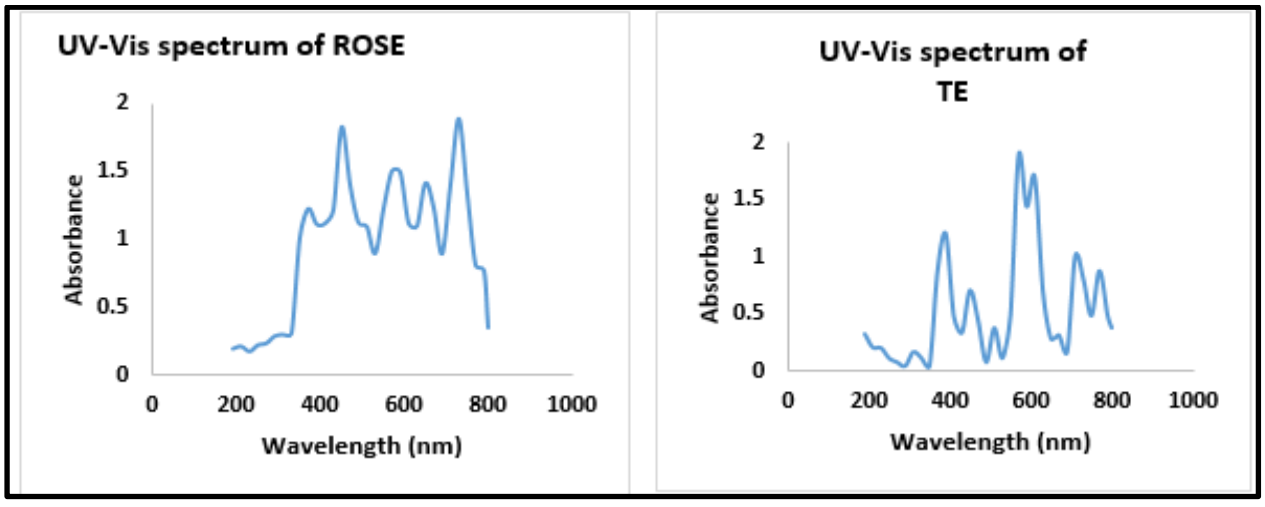
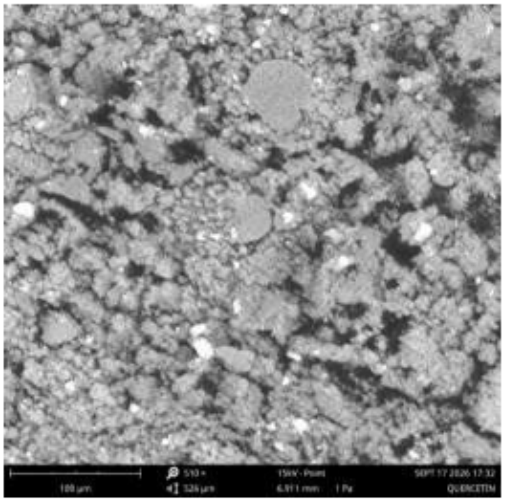



***Fig. 3.2*** *UV-Vis spectrum of ROSE and TE.*

For TE, the spectrum showed prominent absorption maxima at approximately 570 and 610 nm, with absorbance values of 1.892 and 1.702, respectively. An additional absorption feature was observed around 390 nm. These absorption features indicate the presence of chromophoric constituents capable of absorbing radiation in the measured wavelength range.

Surface Morphology and Elemental Composition of the Extracts: The surface morphologies and elemental compositions of ROSE and TE were examined using scanning electron microscopy coupled with energy-dispersive X-ray spectroscopy (SEM–EDX). The SEM micrographs and corresponding EDX results are presented below. In Figure 3.3a, the ROSE

micrograph reveals an irregular and heterogeneous surface structure characterized by aggregated particles and unevenly distributed flakes. The observed morphology suggests that the extract consists of several particulate organic constituents with varying surface features. The EDX analysis shows that carbon is the predominant detected element, accounting for 63.11 atomic %, while oxygen represents 22.40 atomic %. Other detected elements include zinc, calcium, iron, potassium, magnesium, silicon, nitrogen, phosphorus, and silver.

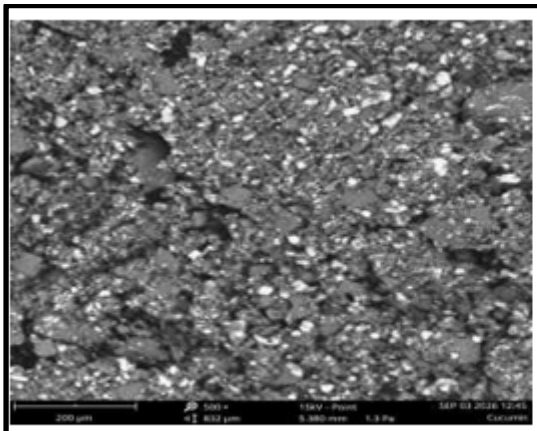


| Element Number | Element Symbol | Element Name | Atomic Conc. | Weight Conc. |
|---|---|---|---|---|
| 8 | O | Oxygen | 22.40 | 34.30 |
| 47 | Ag | Silver | 0.90 | 2.10 |
| 30 | Zn | Zinc | 2.01 | 2.30 |
| 26 | Fe | Iron | 1.11 | 2.10 |
| 15 | P | Phosphorus | 0.03 | 0.07 |
| 13 | Al | Aluminium | 0.00 | 0.00 |
| 22 | Ti | Titanium | 0.00 | 0.00 |
| 17 | Cl | Chlorine | 0.00 | 0.00 |
| 6 | C | Carbon | 63.11 | 58.20 |
| 14 | Si | Silicon | 1.20 | 0.01 |
| 20 | Ca | Calcium | 2.03 | 1.01 |
| 19 | K | Potassium | 1.11 | 0.02 |
| 12 | Mg | Magnesium | 1.20 | 0.04 |
| 7 | N | Nitrogen | 2.10 | 0.10 |

**SEM-EDX micrograph of ROSE**

***Fig. 3.3a*** *SEM-EDX micrograph of ROSE*

The SEM micrograph of TE as shown in Figure 3.3b, reveals a heterogeneous structure characterized by dense granular aggregates, irregular particles, and visible surface voids. The morphology indicates the presence of aggregated particulate constituents within the crude extract. Its EDX spectrum shows carbon as the predominant detected element, accounting for 55.03 atomic %, while oxygen constitutes 37.38 atomic %. Minor quantities of other elements, including iron, zinc, silver, phosphorus, silicon, and nitrogen, were also detected.



| Element Number | Element Symbol | Element Name | Atomic Conc. | Weight Conc. |
|---|---|---|---|---|
| 8 | O | Oxygen | 37.38 | 31.03 |
| 47 | Ag | Silver | 1.20 | 0.20 |
| 30 | Zn | Zinc | 3.10 | 0.70 |
| 26 | Fe | Iron | 1.44 | 1.02 |
| 15 | P | Phosphorus | 1.21 | 1.01 |
| 13 | Al | Aluminium | 0.00 | 0.04 |
| 22 | Ti | Titanium | 0.00 | 0.00 |
| 17 | Cl | Chlorine | 0.00 | 0.00 |
| 6 | C | Carbon | 55.03 | 59.07 |
| 14 | Si | Silicon | 0.11 | 0.00 |
| 20 | Ca | Calcium | 0.00 | 0.00 |
| 19 | K | Potassium | 0.00 | 0.00 |
| 12 | Mg | Magnesium | 0.00 | 0.00 |
| 7 | N | Nitrogen | 0.01 | 0.10 |

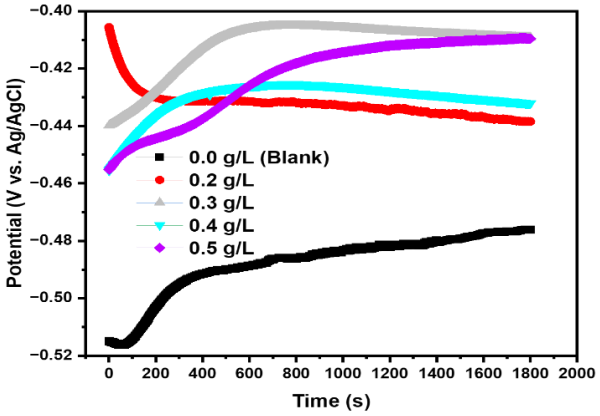
**SEM-EDX micrograph of TE**

***Fig. 3.3b*** *SEM-EDX micrograph of TE.*

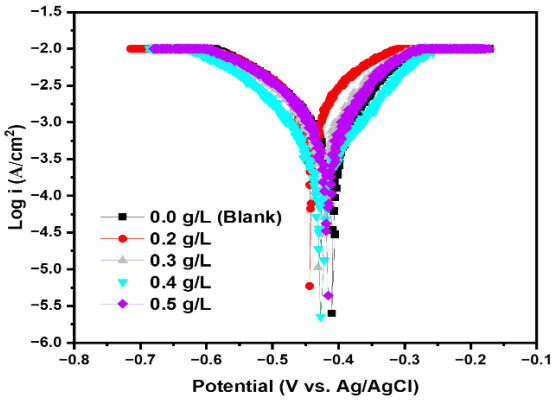
The predominance of carbon and oxygen in both extracts indicates that their detected elemental compositions are largely associated with organic constituents. Carbon forms the structural framework of the major phytochemical compounds, while oxygen is associated with functional groups such as hydroxyl, carbonyl, ether, and other oxygen-containing groups. These groups are chemically relevant to the possible adsorption behaviour of the extracts during corrosion inhibition.

Electrochemical Evaluation of the Corrosion Inhibition Performance of ROSE and TE: The corrosion inhibition performance of red onion skin extract (ROSE) and turmeric extract (TE) was investigated using open-circuit potential (OCP), potentiodynamic polarisation (PDP) and electrochemical impedance spectroscopy (EIS). The experiments were conducted using mild steel in 1 M HCl at room temperature, with inhibitor concentrations ranging from 0.2 to 0.5 g/L. These electrochemical techniques provide complementary information on the stability of the metal–solution interface, the kinetics of the anodic and cathodic corrosion reactions, and the resistance developed following the introduction of inhibitor constituents (Dehghani *et al.,* 2020; Holla *et al.,* 2024).

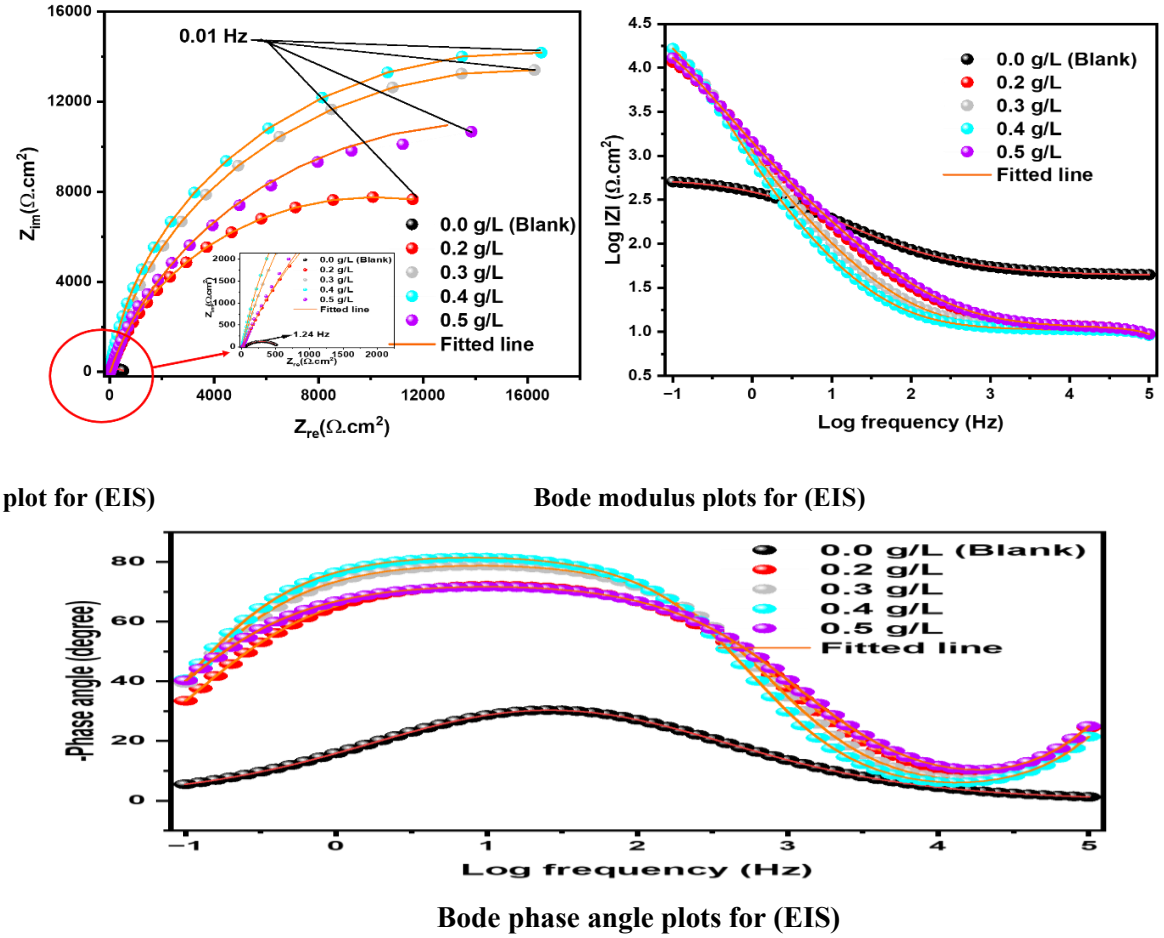
Corrosion Inhibition Performance of Red Onion Skin Quercetin-Rich Extract (ROSE): The electrochemical responses of mild steel in 1 M HCl in the absence and presence of different concentrations of ROSE are presented in Figure 3.4. The OCP curves show changes in electrode potential following the introduction of the extract, indicating modifications in the electrochemical environment at the metal–solution interface. The PDP curves further reveal a substantial reduction in both anodic and cathodic current densities, suggesting that ROSE suppresses iron dissolution and cathodic hydrogen evolution. The corresponding corrosion parameters presented in Table 3.5 show that the corrosion current density decreased considerably from 1816 μA $cm^{-2}$ in the uninhibited solution to 71, 34, 32 and 56 μA $cm^{-2}$ at ROSE concentrations of 0.2, 0.3, 0.4 and 0.5 g/L, respectively. The corresponding inhibition efficiencies were 96.09, 98.13, 98.24 and 96.92%, with the highest efficiency of 98.24% obtained at 0.4 g/L. The corrosion potential shifted from −406 mV for the blank solution to values between −442 and −415 mV in the inhibited systems. The maximum potential displacement of 36 mV is below the commonly applied 85 mV criterion for distinguishing predominantly anodic or cathodic inhibitors. This indicates that ROSE functions as a mixed-type corrosion inhibitor, influencing both anodic metal dissolution and cathodic hydrogen evolution. The considerable decrease in corrosion current density demonstrates the ability of the extract to reduce the overall corrosion reaction, most likely through adsorption of its constituent phytochemicals on the steel surface. Such adsorption can progressively reduce the number of electrochemically active sites available for corrosion reactions (Dehghani *et al.,* 2020; Hijazi *et al.,* 2021).




**Open circuit potential (OCP) analysis**




**Potentiodynamic polarization (PDP)**




**Nyquist plot for (EIS)** **Bode modulus plots for (EIS)**

**Bode phase angle plots for (EIS)**

***Fig. 3:4*** *Open circuit potential (OCP) analysis, Potentiodynamic polarisation (PDP) analysis, Nyquist plot for electrochemical impedance spectroscopy (EIS) analysis, Bode modulus plots for electrochemical impedance spectroscopy (EIS) analysis, and Bode phase angle plots for electrochemical impedance spectroscopy (EIS) analysis of mild steel for blank uninhibited system in comparison with the different concentrations of ROSE inhibitor, tested in 1M HCl corrosive environment at room temperature.*

The EIS responses of mild steel in the presence of ROSE are also presented in Figure 3.4. The enlarged capacitive arcs in the Nyquist plots indicate an increase in resistance to charge transfer across the metal–solution interface. The higher impedance response in the Bode modulus plots suggests improved resistance of the steel surface to the corrosive environment, while changes in the Bode phase-angle profiles indicate modifications in interfacial capacitive behaviour. The impedance parameters in Table 3.6 show that Rct increased from 450.78 Ω $cm^2$ for the uninhibited system to 17,000.61, 29,000.33, 31,200.21 and 22,200.73 Ω $cm^2$ at ROSE concentrations of 0.2, 0.3, 0.4 and 0.5 g/L, respectively. The corresponding EIS inhibition efficiencies are 97.35, 98.45, 98.56 and 97.97%, respectively. The highest efficiency (98.56%) was therefore obtained at 0.4 g/L. The increase in Rct indicates that ROSE impedes the interfacial charge-transfer process associated with corrosion. The impedance response is consistent with the development of an inhibiting interfacial layer that limits interaction between the corrosive solution and the steel surface. Changes in the constant-phase-element parameters also indicate modifications in the interfacial capacitive properties following inhibitor addition (Holla *et al.,* 2024).

Table 3.5: Potentiodynamic polarisation parameters for mild steel in uninhibited 1 M HCl and 1 M HCl containing different concentrations of ROSE.

| System (1 M HCl) | $E_{corr}$ mV/Ag/AgCl | $I_{corr}$ μAcm$^{-2}$ | Ba mVdec$^{-1}$ | βc mVdec$^{-1}$ | Θ | IE % |
|---|---|---|---|---|---|---|
| **0.0 g/L** | -406 | 1816 | 104 | 106 | - | - |
| **0.2 g/L** | -442 | 71 | 92 | 101 | 0.961 | 96.09 |
| **0.3 g/L** | -429 | 34 | 76 | 85 | 0.981 | 98.13 |
| **0.4 g/L** | -426 | 32 | 56 | 76 | 0.982 | 98.24 |
| **0.5 g/L** | -415 | 56 | 54 | 45 | 0.969 | 96.92 |

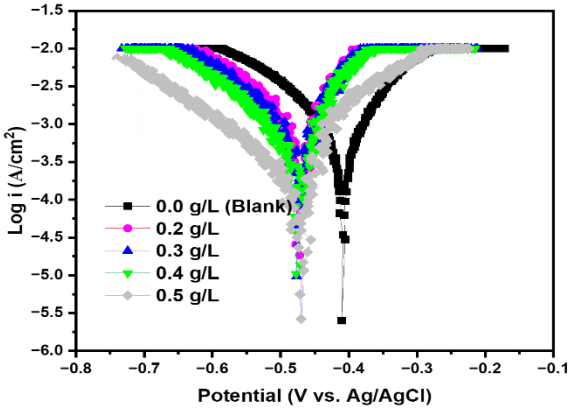
Table 3.6: Electrochemical impedance spectroscopy (EIS) parameters for mild steel in uninhibited 1 M HCl and 1 M HCl containing different concentrations of ROSE.

| System (1 M HCl) | $R_s$ (Ω. cm$^2$) | $R_{po}$ (Ω. cm$^2$) | Q1x10$^{-5}$ (μΩ$^{-1}$ $s^n$ cm$^{-2}$) | n1 | $R_{ct}$ (Ω cm$^2$) | Q2x10$^{-5}$ (μΩ$^{-1}$ $s^n$ cm$^{-2}$) | n2 | Θ | IE % |
|---|---|---|---|---|---|---|---|---|---|
| **0.0 g/L** | 18.30 | 70.58 | 98.52 | 0.88 | 450.78 | 92.75 | 0.86 | - | - |
| **0.2 g/L** | 20.26 | 400.39 | 78.32 | 0.89 | 17000.61 | 74.43 | 0.88 | 0.973 | 97.35 |
| **0.3 g/L** | 20.32 | 1100.44 | 65.88 | 0.97 | 29000.33 | 66.82 | 0.94 | 0.984 | 98.45 |
| **0.4 g/L** | 20.72 | 2000.82 | 60.46 | 0.98 | 31200.21 | 58.68 | 0.88 | 0.986 | 98.56 |
| **0.5 g/L** | 21.55 | 900.59 | 55.77 | 0.98 | 22200.73 | 54.26 | 0.99 | 0.980 | 97.97 |

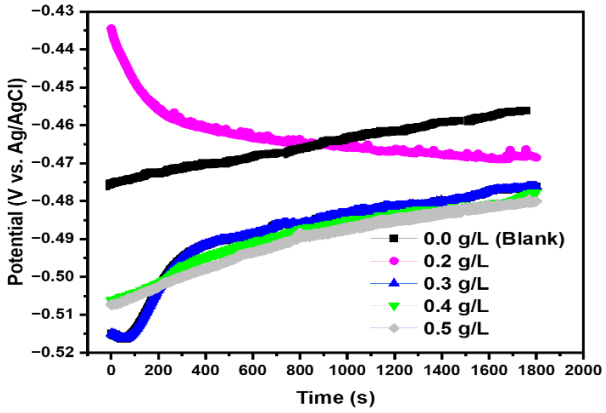
The inhibition behaviour of ROSE can be associated with its phytochemical composition, particularly its quercetin content of 34.4772 μg/mL, which was the predominant quantified constituent of the extract. Quercetin is a polyphenolic flavonoid containing several hydroxyl groups, aromatic rings and carbonyl functionality. These structural features provide potential interaction sites through which the molecule can adsorb onto the steel surface. The oxygen-containing functional groups and conjugated aromatic system may facilitate interactions with the metal surface, contributing to the formation of an adsorbed organic layer. Such a layer can restrict the access of aggressive species, particularly hydrogen ions, to the active sites of the metal and consequently reduce both anodic and cathodic corrosion reactions. The effectiveness of quercetin as a corrosion-inhibiting constituent has also been demonstrated through electrochemical and computational investigations of mild steel in acidic environments, where its adsorption was associated with mixed-type inhibition and the development of a protective surface film (Dehghani *et al.,* 2020). Therefore, the high inhibition efficiencies obtained from the PDP and EIS measurements in the present study indicate that the quercetin-rich ROSE provides effective protection against mild steel corrosion in 1 M HCl.

Corrosion Inhibition Performance of Turmeric Extract (TE): The electrochemical responses of mild steel in 1 M HCl in the absence and presence of different concentrations of TE are presented in Figure 3.5. The OCP curves show changes in electrode potential following the introduction of the extract, indicating modifications in the electrochemical conditions at the metal–solution interface. The PDP curves further reveal reductions in both anodic and cathodic current densities, demonstrating that TE inhibits the electrochemical reactions responsible for mild steel corrosion. The corresponding corrosion parameters presented in Table 3.7 show that the corrosion current density decreased from 1816 μA cm$^{-2}$ in the uninhibited solution to 321, 250, 49 and 50 μA cm$^{-2}$ at TE concentrations of 0.2, 0.3, 0.4 and 0.5 g/L, respectively. The corresponding inhibition efficiencies were 82.32, 86.23, 97.30 and 97.25%, respectively, with the highest PDP inhibition efficiency of 97.30% obtained at 0.4 g/L. The corrosion potential shifted from −406 mV for the blank solution to values between −470 and −476 mV in the inhibited systems. The maximum potential displacement of 70 mV remains below the commonly applied 85 mV criterion, indicating that TE also functions as a mixed-type corrosion inhibitor, although the negative displacement suggests a noticeable cathodic tendency. This implies that the extract influences both iron dissolution and hydrogen evolution, with a more pronounced effect on the cathodic

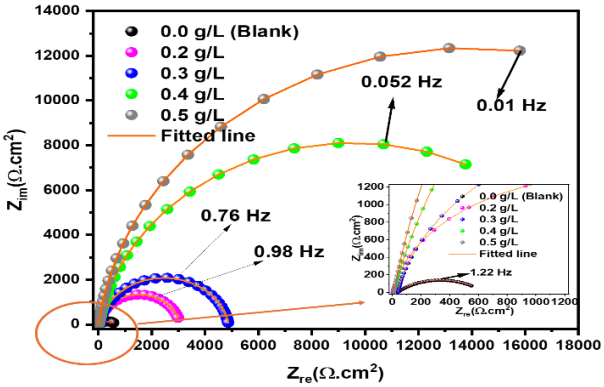
reaction. The substantial reduction in corrosion current density, particularly at concentrations of 0.4 and 0.5 g/L, indicates improved suppression of the overall corrosion process. This behaviour suggests that increasing the concentration of TE enhances the availability of its active constituents for adsorption onto the steel surface, thereby restricting the electrochemical reactions responsible for corrosion. The classification and interpretation are consistent with the electrochemical approach used to identify mixed-type inhibition in plant-derived corrosion inhibitors (Dehghani *et al.,* 2020; Chidiebere *et al.,* 2024).



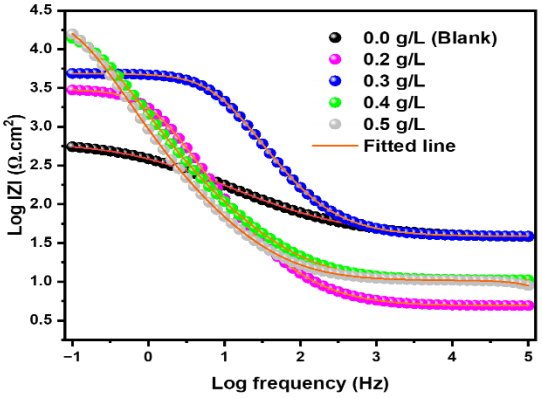

**Open circuit potential (OCP) analysis**



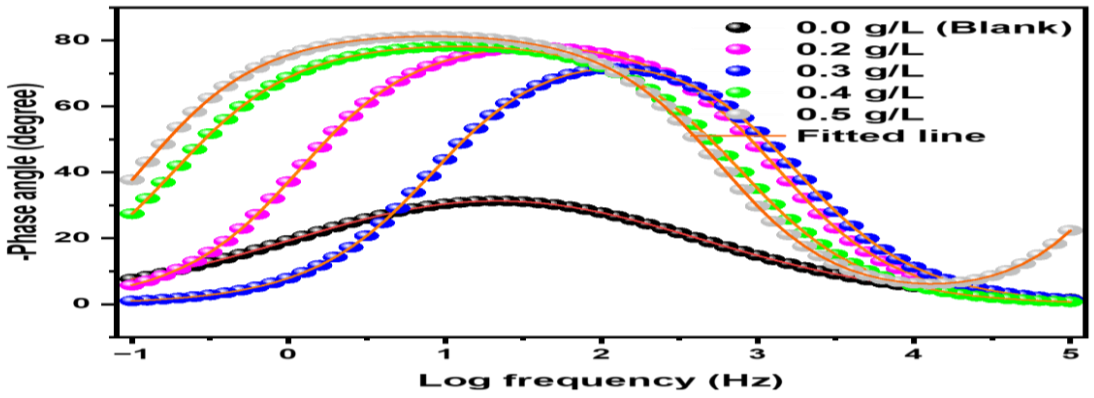

**Potentiodynamic polarization (PDP) analysis**




**Nyquist plot for EIS**




**Bode modulus plots for EIS**




**Bode phase angle plots for EIS**

***Fig. 3.5*** *Open circuit potential (OCP) analysis, Potentiodynamic polarisation (PDP) analysis, Nyquist plot for electrochemical impedance spectroscopy (EIS) analysis, Bode modulus plots for electrochemical impedance spectroscopy (EIS) analysis, and Bode phase angle plots for electrochemical impedance spectroscopy (EIS) analysis of mild steel for blank uninhibited system in comparison with the different concentrations of TE inhibitor, tested in 1M HCl corrosive environment at room temperature.*

Further evidence of the protective action of TE is provided by the EIS responses in Figure 3.5. The increase in the diameter of the capacitive arcs in the Nyquist plots indicates improved resistance to charge transfer at the metal–solution interface. The higher impedance response in the Bode modulus plots suggests a reduction in the electrochemical activity of the steel surface, while changes in the Bode phase-angle profiles indicate modifications in interfacial capacitive behaviour. The impedance parameters in Table 3.8 show that Rct increased from 450.28 Ω $cm^2$ for the uninhibited system to 3,000.83, 4,000.44, 18,000.37 and 23,000.53 Ω $cm^2$ at TE concentrations of 0.2, 0.3, 0.4 and 0.5 g/L, respectively. The EIS inhibition efficiencies are 84.99, 88.74, 97.50 and 98.04%, respectively. The highest efficiency (98.04%) was therefore obtained at 0.5 g/L. The progressive increase in Rct indicates that TE increasingly impedes charge transfer associated with the corrosion process. Changes in the constant-phase-element parameters further suggest modifications in the capacitive characteristics of the metal–solution interface following adsorption of extract constituents (Holla *et al.,* 2024).

Table 3.7: Potentiodynamic polarisation parameters for mild steel in uninhibited 1 M HCl and 1 M HCl containing different concentrations of TE.

| **System (1 M HCl)** | **$E_{corr}$** | **$I_{corr}$** | **Ba** | **Bc** | **θ** | **IE** |
|---|---|---|---|---|---|---|
| | **mV/Ag/AgCl** | **μAcm$^{-2}$** | **mVdec$^{-1}$** | **mVdec$^{-1}$** | | **%** |
| **0.0 g/L** | -406 | 1816 | 105 | 121 | - | - |
| **0.2 g/L** | -470 | 321 | 99 | 101 | 0.823 | 82.32 |
| **0.3 g/L** | -476 | 250 | 84 | 94 | 0.862 | 86.23 |
| **0.4 g/L** | -476 | 49 | 71 | 80 | 0.973 | 97.30 |
| **0.5 g/L** | -475 | 50 | 61 | 69 | 0.973 | 97.25 |

Table 3.8: Electrochemical impedance spectroscopy (EIS) parameters for mild steel in uninhibited 1 M HCl and 1 M HCl containing different concentrations of TE.

| **System (1 M HCl)** | **$R_s$ (Ω. $cm^2$)** | **$R_{po}$ (Ω. $cm^2$)** | **Q1x10$^{-5}$ (μΩ$^{-1}$ s$^n$ cm$^{-2}$)** | **n1** | **$R_{ct}$ (Ω $cm^2$)** | **Q2x10$^{-5}$ (μΩ$^{-1}$ s$^n$ cm$^{-2}$)** | **n2** | **θ** | **IE %** |
|---|---|---|---|---|---|---|---|---|---|
| **0.0 g/L** | 19.01 | 70.32 | 90.39 | 0.88 | 450.28 | 95.38 | 0.88 | - | - |
| **0.2 g/L** | 20.14 | 100.47 | 82.64 | 0.89 | 3000.83 | 85.62 | 0.88 | 0.850 | 84.99 |
| **0.3 g/L** | 20.26 | 500.88 | 77.04 | 0.89 | 4000.44 | 65.62 | 0.98 | 0.887 | 88.74 |
| **0.4 g/L** | 20.28 | 1200.73 | 61.82 | 0.95 | 18000.37 | 55.54 | 0.99 | 0.975 | 97.50 |
| **0.5 g/L** | 21.11 | 1300.31 | 45.32 | 0.98 | 23000.53 | 48.53 | 0.98 | 0.980 | 98.04 |

The inhibition performance of TE can be related to its phytochemical composition, particularly its curcumin content of 40.2159 µg/mL, which was the predominant quantified constituent. Curcumin possesses phenolic hydroxyl groups, methoxy substituents and a conjugated β-diketone structure containing carbonyl groups. These features provide potential sites for interaction with the steel surface. Adsorption of curcumin and other organic constituents may promote an inhibiting film that reduces direct contact between the metal and the corrosive solution. The resulting surface coverage can restrict the access of aggressive species to active metal sites and impede both anodic and cathodic corrosion reactions. Electrochemical investigations of *Curcuma longa* root extract have similarly reported inhibition of mild steel corrosion in hydrochloric acid through a mixed-type mechanism (Chidiebere *et al.,* 2024). The present results indicate that curcumin-rich TE reduces mild steel corrosion in 1 M HCl.

**Comparative Evaluation of Quercetin-Rich ROSE and Curcumin-Rich TE**

The comparative phytochemical results establish the quercetin-rich and curcumin-rich characteristics of the extracts. Quercetin was the predominant quantified constituent of ROSE, at 34.4772 µg/mL, representing approximately 59.82% of its total quantified phytochemicals (57.6338 µg/mL). Similarly, curcumin accounted for 40.2159 µg/mL of the total quantified constituents in TE (65.8602 µg/mL), representing approximately 61.04%. Although TE recorded a higher total quantified phytochemical concentration, both extracts contained their respective major constituents in substantial proportions. These polyphenolic compounds contain oxygen-bearing functional groups and conjugated structures that may provide adsorption centres for interaction with metallic surfaces (Kumar, H. *et al.,* 2022; Kumar, M. *et al.,* 2022; Saranya *et al.,* 2024).

The physicochemical results showed that both extracts were soluble in the tested organic solvents but insoluble in water. Their melting ranges were 78–102.40 °C for ROSE and 89–107.50 °C for TE. The FTIR spectra (Figure 3.1) revealed hydroxyl, aromatic and C–O-related functional groups in both extracts. ROSE exhibited prominent O–H absorption bands at 3542.60 and 3239.52 $cm^{-1}$, whereas TE showed corresponding bands at 3357.86, 3200.96 and 3146.89 $cm^{-1}$. The absorption at 1614.31 $cm^{-1}$ in TE was associated with conjugated carbonyl and aromatic C=C vibrations, supporting the presence of oxygen-containing and conjugated structures associated with curcumin. Such functional groups are relevant to the adsorption behaviour of organic corrosion inhibitors (Ahamed *et al.,* 2019; Anadebe *et al.,* 2018; Ramezanzadeh *et al.,* 2019).

The UV–Vis spectra (Figure 3.2) further distinguished the extracts. ROSE exhibited absorption maxima around 450 and 730 nm, while TE showed maxima around 570 and 610 nm, with an additional feature near 390 nm. These features reflect differences in the chromophoric constituents of the extracts. The SEM–EDX results Figure 3.3 (a & b) also revealed distinct heterogeneous morphologies. ROSE consisted of irregular aggregated particles and unevenly distributed flakes, whereas TE displayed dense granular aggregates, irregular particles and visible surface voids. Carbon and oxygen were the predominant detected elements in both extracts, with atomic concentrations of 63.11% and 22.40% for ROSE and 55.03% and 37.38% for TE, respectively. These observations support the presence of organic constituents containing oxygen-bearing functional groups. However, the SEM–EDX results describe the extracts themselves and do not constitute direct evidence of protective films on the steel surface.

The electrochemical results provide further evidence of the corrosion-inhibition performance of both extracts. The individual OCP, PDP and EIS responses are presented in Figures 3.4 and 3.5, while their corresponding parameters are reported in Tables 3.5–3.8. For ROSE, the corrosion current density decreased from 1816 µA $cm^{-2}$ in the uninhibited solution to 32 µA $cm^{-2}$ at 0.4 g/L, producing the highest PDP inhibition efficiency of 98.24%. TE also reduced the corrosion current density considerably, reaching 49 µA $cm^{-2}$ at 0.4 g/L, with a maximum PDP inhibition efficiency of 97.30%. The comparative PDP inhibition efficiencies are presented in Figure 3.6. ROSE exhibited higher efficiencies at 0.2, 0.3 and 0.4 g/L, whereas TE recorded a slightly higher value at 0.5 g/L. The maximum negative corrosion-potential displacement was 36 mV for ROSE and 70 mV for TE. Since both values are below the commonly applied 85 mV criterion, both extracts are classified as mixed-type inhibitors, although TE exhibited a more noticeable cathodic

tendency. Mixed-type behaviour has also been reported for several plant-derived corrosion inhibitors evaluated using polarisation measurements (Gadow & Fakeeh, 2022; Ishak *et al.,* 2019; Deyab *et al.,* 2022).

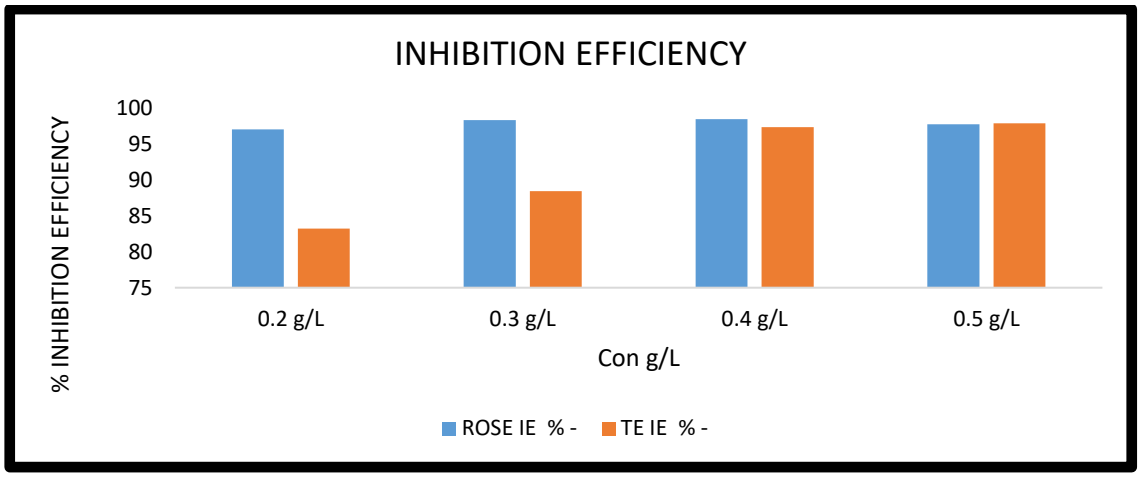



***Fig. 3.6*** *Comparative potentiodynamic polarisation inhibition efficiencies of quercetin-rich ROSE and curcumin-rich TE at different inhibitor concentrations.*

The EIS results further support the protective action of the extracts. For ROSE, Rct increased from 450.78 Ω $cm^2$ in the blank solution to 31,200.21 Ω $cm^2$ at 0.4 g/L. For TE, Rct increased from 450.28 Ω $cm^2$ to 23,000.53 Ω $cm^2$ at 0.5 g/L. The maximum EIS inhibition efficiencies of 98.56% for ROSE at 0.4 g/L and 98.04% for TE at 0.5 g/L. ROSE showed higher efficiencies at 0.2, 0.3 and 0.4 g/L, while TE recorded a slightly higher value at 0.5 g/L. The increase in Rct and Rpo, accompanied by changes in the CPE parameters, indicates modifications in the interfacial electrochemical properties following inhibitor addition. These changes are consistent with adsorption of organic constituents and the development of an inhibiting interfacial layer (Berrissoul *et al.,* 2020a, 2020b; Manh *et al.,* 2022; Marhamati *et al.,* 2021).

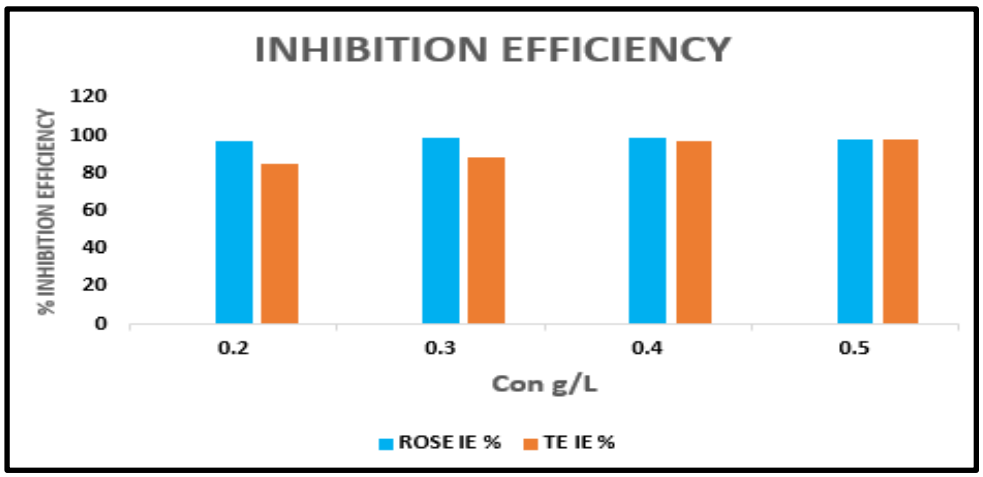



***Fig. 3.7*** *Comparative electrochemical impedance spectroscopy inhibition efficiencies of quercetin-rich ROSE and curcumin-rich TE at different inhibitor concentrations.*

**Table 3.9:** Comparative summary of the physicochemical, spectroscopic and corrosion-inhibition characteristics of quercetin-rich ROSE and curcumin-rich TE

| Characteristic | Quercetin-rich ROSE | Curcumin-rich TE |
|---|---|---|

| Major phytochemical | Quercetin | Curcumin |
|---|---|---|
| Major constituent concentration (μg/mL) | 34.4772 | 40.2159 |
| Total quantified phytochemicals (μg/mL) | 57.6338 | 65.8602 |
| Major constituent proportion (%) | 59.82 | 61.04 |
| Melting range (°C) | 78–102.40 | 89–107.50 |
| Principal FTIR features ($cm^{-1}$) | 3542.60, 3239.52, 3120.70, 2901.12, 1411.90, 1284.82 | 3357.86, 3200.96, 3146.89, 2962.15, 2861.01, 1614.31, 1544.81, 1357.99, 1265.08 |
| UV–Vis absorption maxima (nm) | 450 and 730 | 570 and 610; additional feature at 390 |
| SEM morphology | Irregular aggregates and uneven flakes | Dense granular aggregates, irregular particles and surface voids |
| Predominant EDX elements (atomic %) | C: 63.11; O: 22.40 | C: 55.03; O: 37.38 |
| Maximum PDP inhibition efficiency (%) | 98.24 at 0.4 g/L | 97.30 at 0.4 g/L |
| Maximum reported EIS inhibition efficiency (%) | 98.56 at 0.4 g/L | 98.04 at 0.5 g/L |
| Maximum Rct (Ω $cm^2$) | 31,200.21 at 0.4 g/L | 23,000.53 at 0.5 g/L |
| Inhibition classification | Mixed-type | Mixed-type |

In conclusion, both quercetin-rich ROSE and curcumin-rich TE demonstrated effective inhibition of mild steel corrosion in 1 M HCl. ROSE showed stronger performance at intermediate concentrations, particularly at 0.4 g/L, where it recorded the highest PDP and EIS inhibition efficiencies. TE also provided substantial protection, with its highest PDP efficiency at 0.4 g/L and its highest EIS efficiency at 0.5 g/L. The differences in performance may be associated with the distinct phytochemical compositions and functional groups of quercetin and curcumin, together with contributions from other extract constituents. Under the conditions investigated, ROSE demonstrated the stronger overall performance at 0.4 g/L.

## CONCLUSION

This study investigated the corrosion inhibition performance of quercetin-rich red onion skin extract (ROSE) and curcumin-rich turmeric extract (TE) on mild steel in 1 M HCl using open-circuit potential, potentiodynamic polarisation and electrochemical impedance spectroscopy. Phytochemical analysis identified quercetin (34.4772 μg/mL) and curcumin (40.2159 μg/mL) as the predominant quantified constituents of ROSE and TE, respectively. FTIR, UV–Vis and SEM–EDX characterisation established the presence of organic constituents containing oxygen-bearing functional groups and conjugated structures that may facilitate interactions with the metal surface. Both extracts demonstrated substantial corrosion-inhibition performance and mixed-type behaviour. ROSE achieved maximum PDP and EIS inhibition efficiencies of 98.24% and 98.56%, respectively, at 0.4 g/L. TE recorded maximum PDP and EIS efficiencies of 97.30% and 98.04%, respectively, at 0.4 and 0.5 g/L. The corresponding increases in charge-transfer resistance further support their inhibiting effects. Overall, ROSE demonstrated stronger inhibition performance, particularly at 0.4 g/L. These findings establish both extracts as promising plant-derived corrosion inhibitors under the experimental conditions investigated.

## CRediT authorship contribution statement

Samson Uchenna Eze: Conceptualization, Investigation, Formal analysis, Data curation, Writing – original draft. Jude, Ebere Kanu: Conceptualization, Investigation, Formal analysis, Writing – original draft. Abosede, Olubunmi James: Supervision, Validation, Writing – review & editing. Ozioma Achugasim: Supervision, Validation, Writing – review &

editing. All authors reviewed and approved the final manuscript; Uche John Chukwu: Supervision, Validation, Writing – review & editing. Onyewuchi Akaranta: Writing – review & editing. Abuchi Elebo: Writing – review & visualization. All authors reviewed and approved the final manuscript.

**Conflict of Interest**
The authors declare that they have no competing interests.

**Data Availability:**
The datasets generated and analyzed during this study are available from the corresponding author upon reasonable request.

**Acknowledgements**
The authors gratefully acknowledge the members of Professor James' Research Group and the staff and management of ACFOR Laboratory, particularly Mr. Teddy Augustine Gboto and Mr. James Daniel Onobun, for their contributions. Special appreciation is extended to Dr. Vitalis Ikenna Chukwuike for his support and assistance during the corrosion studies.

**Declaration of Generative AI and AI-Assisted Technologies**
During the preparation of this work, the authors used Grammarly to assist with language editing, grammar correction, and improvement of readability. After using this tool, the authors reviewed and edited the content as needed and take full responsibility for the content of the published article.

**REFERENCES**

Adama, K. K., & Onyeachu, B. I. (2023). Inhibitory action of *Spondias mombin* leaves extracts on corrosion of mild steel in 1 M HCl. *Nigerian Journal of Technological Development, 20*(1), 15–24. https://doi.org/10.63746/njtd.v20i1.1294

Ahamed, K. R., Farzana, B. A., Diraviam, S. J., Dorothy, R., Rajendran, S., & Al-Hashem, A. (2019). Mild steel corrosion inhibition by the aqueous extract of *Commelina benghalensis* leaves. *Portugaliae Electrochimica Acta, 37*(1), 51–70. https://doi.org/10.4152/pea.201901051

Al-Ansari, M. M., Al-Humaid, L., Aldawsari, M., Abid, I. F., Jhanani, G. K., & Shanmuganathan, R. (2023). Quercetin extraction from small onion skin (*Allium cepa L.* var. aggregatum Don.) and its antioxidant activity. Environmental Research, 224, Article 115497. https://doi.org/10.1016/j.envres.2023.115497

Anadebe, V. C., Onukwuli, O. D., Omotioma, M., & Okafor, N. A. (2018). Optimization and electrochemical study on the control of mild steel corrosion in hydrochloric acid solution with bitter kola leaf extract as inhibitor. *South African Journal of Chemistry, 71*, 51–63. https://doi.org/10.17159/0379-4350/2018/v71a7

Benabdallah, G. A., Kouri, H., Labjar, N., Bouiti, K., Bouissoui, E. M., Dahrouch, A., & El Hajjaji, S. (2023). Eco-friendly *Pistacia lentiscus* leaves extract corrosion inhibitor for C38 steel in 1 M HCl. *International Journal of Corrosion and Scale Inhibition, 12*(1), 292–308. https://doi.org/10.17675/2305-6894-2023-12-1-17

Berrissoul, A., Loukili, E., Mechbal, N., Benhiba, F., Guenbour, A., Dikici, B., Zarrouk, A., & Dafali, A. (2020a). Anticorrosion effect of a green sustainable inhibitor on mild steel in hydrochloric acid. *Journal of Colloid and Interface Science, 580*, 740–752. https://doi.org/10.1016/j.jcis.2020.07.073

Berrissoul, A., Ouarhach, A., Benhiba, F., Romane, A., Zarrouk, A., Guenbour, A., Dikici, B., & Dafali, A. (2020b). Evaluation of *Lavandula mairei* extract as green inhibitor for mild steel corrosion in 1 M HCl solution: Experimental and

theoretical approach. *Journal of Molecular Liquids, 313*, Article 113493. https://doi.org/10.1016/j.molliq.2020.113493

Boscariol, R., Paulino, T. H., Oliveira, J. M., Jr., Balcão, V. M., & Vila, M. M. D. C. (2022). Characterization of commercially available turmeric for use in pharmaceutical products and food supplements. *Journal of the Brazilian Chemical Society, 33*(12), 1392–1401. https://doi.org/10.21577/0103-5053.20220073

Chadorshabi, S., Hallaj-Nezhadi, S., & Ghasempour, Z. (2022). Red onion skin active ingredients, extraction and biological properties for functional food applications. *Food Chemistry, 386*, Article 132737. https://doi.org/10.1016/j.foodchem.2022.132737

Chidiebere, M. A., Anadebe, V. C., & Barik, R. C. (2024). Insight into the corrosion resistance of mild steel in an acidic environment in the presence of an organic extract: Experimental and computational approach. *Results in Engineering, 23*, Article 102787. https://doi.org/10.1016/j.rineng.2024.102787

Dehghani, A., Mostafatabar, A. H., Bahlakeh, G., Ramezanzadeh, B., & Ramezanzadeh, M. (2020). Detailed-level computer modeling explorations complemented with comprehensive experimental studies of quercetin as a highly effective inhibitor for acid-induced steel corrosion. *Journal of Molecular Liquids, 316*, 113035. https://doi.org/10.1016/j.molliq.2020.113035

Deyab, M. A., Mohsen, Q., & Guo, L. (2022). Theoretical, chemical, and electrochemical studies of *Equisetum arvense* extract as an impactful inhibitor of steel corrosion in 2 M HCl electrolyte. *Scientific Reports, 12*, Article 2255. https://doi.org/10.1038/s41598-022-06215-6

Doumane, G., Bensalah, J., Ouakki, M., Aribou, Z., Boussalem, O., Mzioud, K., Safi, Z. S., Berisha, A., Bourhia, M., Gaafar, A.-R. Z., Ibenmoussa, S., Wondmie, G. F., Zarrouk, A., Ebn Touhami, M., & Habsaoui, A. (2024). Alkaloid extract of seed *Citrullus colocynthis* as novel green inhibitor for mild steel corrosion in one molar HCl acid solution: DFT and MC/MD approaches. *Scientific Reports, 14*, Article 16857. https://doi.org/10.1038/s41598-024-67011-y

Emmanuel, J. K. (2024). Corrosion protection of mild steel in corrosive media, a shift from synthetic to natural corrosion inhibitors: A review. *Bulletin of the National Research Centre, 48*, Article 26. https://doi.org/10.1186/s42269-024-01181-7

Ferreira, E. S., Giacomelli, C., Giacomelli, F. C., & Spinelli, A. (2004). Evaluation of the inhibitor effect of L-ascorbic acid on the corrosion of mild steel. *Materials Chemistry and Physics, 83*(1), 129–134. https://doi.org/10.1016/j.matchemphys.2003.09.020

Ferreira, K. C. R., Cordeiro, R. F. B., Nunes, J. C., Orofino, H., Magalhães, M., Torres, A. G., & D'Elia, E. (2016). Corrosion inhibition of carbon steel in HCl solution by aqueous brown onion peel extract. *International Journal of Electrochemical Science, 11*(1), 406–418. https://doi.org/10.1016/S1452-3981(23)15853-6

Gadow, H. S., & Fakeeh, M. (2022). Green inhibitor of carbon steel corrosion in 1 M hydrochloric acid: *Eruca sativa* seed extract (experimental and theoretical studies). *RSC Advances, 12*, 8953–8986. https://doi.org/10.1039/D2RA01296K

Hijazi, K. M., Abdel-Gaber, A. M., Younes, G. O., & Habchi, R. (2021). Comparative study of the effect of an acidic anion on the mild steel corrosion inhibition using *Rhus coriaria* plant extract and its quercetin component. *Portugaliae Electrochimica Acta, 39*(4), 237–252.

Hjouji, K., Ech-chihbi, E., Atemni, I., Ouakki, M., Taleb, M., Ainane, T., & Rais, Z. (2023). Datura stramonium plant seed extracts as a new green corrosion inhibitor for mild steel in 1M HCl solution: Experimental and surface characterisation studies. Sustainable Chemistry and Pharmacy, 34, Article 101170. https://doi.org/10.1016/j.scp.2023.101170

Holla, B. R., Mahesh, R., Manjunath, H. R., & Anjanapura, V. R. (2024). Plant extracts as green corrosion inhibitors for different kinds of steel: A review. *Heliyon, 10*(14), e33748. https://doi.org/10.1016/j.heliyon.2024.e33748

Ishak, A., Adams, F. V., Madu, J. O., Joseph, I. V., & Olubambi, P. A. (2019). Corrosion inhibition of mild steel in 1 M HCl using *Haematostaphis barteri* leaves extract. *Procedia Manufacturing, 35*, 1279–1285. https://doi.org/10.1016/j.promfg.2019.06.088

Jha, V. K., Chauhan, M. S., Pal, S., Jana, S., Ji, G., & Prakash, R. (2022). Experimental and DFT analysis of onion peels for its inhibition behaviour against mild steel corrosion in chloride solutions. Journal of the Indian Chemical Society, 99(7), Article 100534. https://doi.org/10.1016/j.jics.2022.100534

Kumar, H., Yadav, V., & Kumari, A. (2022). Adsorption, corrosion inhibition mechanism, and computational studies of *Azadirachta indica* extract for protecting mild steel: Sustainable and green approach. *Journal of Physics and Chemistry of Solids, 165*, Article 110690. https://doi.org/10.1016/j.jpcs.2022.110690

Kumar, H., Yadav, V., Anu, Saha, S. K., & Kang, N. (2021). Adsorption and inhibition mechanism of efficient and environment friendly corrosion inhibitor for mild steel: Experimental and theoretical study. *Journal of Molecular Liquids, 338*, Article 116634. https://doi.org/10.1016/j.molliq.2021.116634

Kumar, M., Barbhai, M. D., Hasan, M., Dhumal, S., Singh, S., Pandiselvam, R., Rais, N., Natta, S., Senapathy, M., Sinha, N., & Amarowicz, R. (2022). Onion (*Allium cepa L.*) peel: A review on the extraction of bioactive compounds, its antioxidant potential, and its application as a functional food ingredient. Journal of Food Science, 87(10), 4289–4311. https://doi.org/10.1111/1750-3841.16297

Manh, T. D., Huynh, T. L., Thi, B. V., Lee, S., Yi, J., & Nguyen Dang, N. (2022). Corrosion inhibition of mild steel in hydrochloric acid environments containing *Sonneratia caseolaris* leaf extract. *ACS Omega, 7*(10), 8874–8886. https://doi.org/10.1021/acsomega.1c07237

Marhamati, F., Mahdavian, M., & Bazgir, S. (2021). Corrosion mitigation of mild steel in hydrochloric acid solution using grape seed extract. *Scientific Reports, 11*, Article 18374. https://doi.org/10.1038/s41598-021-97944-7

Medupin, R. O., Ukoba, K. O., Yoro, K. O., & Jen, T.-C. (2023). Sustainable approach for corrosion control in mild steel using plant-based inhibitors: A review. *Materials Today Sustainability, 22*, Article 100373. https://doi.org/10.1016/j.mtsust.2023.100373

Miralrio, A., & Espinoza Vázquez, A. (2020). Plant extracts as green corrosion inhibitors for different metal surfaces and corrosive media: A review. *Processes, 8*(8), Article 942. https://doi.org/10.3390/pr8080942

Nikolaychuk, P. A., Zhernakova, A. O., & Enova, Y. A. (2023). Sustainable corrosion inhibition of mild steel in hydrochloric acid using extracts of *Phaseolus vulgaris* and *Vicia faba*. *Annales de Chimie – Science des Matériaux, 47*(6), 405–410. https://doi.org/10.18280/acsm.470607

Ong, C. C., & Karim, K. A. (2017). Inhibitory effect of red onion skin extract on the corrosion of mild steel in acidic medium. *Chemical Engineering Transactions, 56*, 913–918. https://doi.org/10.3303/CET1756153

Ramezanzadeh, M., Bahlakeh, G., Sanaei, Z., & Ramezanzadeh, B. (2019). Corrosion inhibition of mild steel in 1 M HCl solution by ethanolic extract of eco-friendly *Mangifera indica* leaves: Electrochemical, molecular dynamics, Monte Carlo and ab initio study. *Applied Surface Science, 463*, 1058–1077. https://doi.org/10.1016/j.apsusc.2018.09.029

Saranya, J., Vagdevi, K., Jyothirmai, B., Anusuya, N., Benhiba, F., Warad, I., & Zarrouk, A. (2024). Application of quercetin as a green inhibitor to prevent mild steel corrosion in the petroleum industry: Experimental and modelling techniques. *Chemical Data Collections, 50*, Article 101125. https://doi.org/10.1016/j.cdc.2024.101125

Sharma, S., Solanki, A. S., & Sharma, S. K. (2024). Anticorrosive action of eco-friendly plant extracts on mild steel in different concentrations of hydrochloric acid. *Corrosion Reviews, 42*(2), 185–201. https://doi.org/10.1515/corrrev-2023-0053

Sheydaei, M. (2024). The use of plant extracts as green corrosion inhibitors: A review. *Surfaces, 7*(2), 380–403. https://doi.org/10.3390/surfaces7020024

Shwetha, K. M., Praveen, B. M., & Devendra, B. K. (2024). A review on corrosion inhibitors: Types, mechanisms, electrochemical analysis, corrosion rate and efficiency of corrosion inhibitors on mild steel in an acidic environment. *Results in Surfaces and Interfaces, 16*, Article 100258. https://doi.org/10.1016/j.rsurfi.2024.100258

Sowmyashree, A. S., Somya, A., Rao, S., Kumar, C. B. P., Al-Romaizan, A. N., Hussein, M. A., Khan, A., Marwani, H. M., & Asiri, A. M. (2023). Potential sustainable electrochemical corrosion inhibition study of *Citrus limetta* on mild steel surface in aggressive acidic media. *Journal of Materials Research and Technology, 24*, 984–994. https://doi.org/10.1016/j.jmrt.2023.02.039

Teng, Y., Zhang, W., Wang, M., Yu, C., Ma, Y., Bian, J., Yang, X., & Zhang, D. (2021). Anthocyanin as sustainable and non-toxic corrosion inhibitor for mild steel in HCl media: Electrochemical, surface morphology and theoretical investigations. *Journal of Molecular Liquids, 344*, Article 117721. https://doi.org/10.1016/j.molliq.2021.117721

Umoren, S. A., Obot, I. B., & Obi-Egbedi, N. O. (2009). Raphia hookeri gum as a potential eco-friendly inhibitor for mild steel in sulfuric acid. *Journal of Materials Science, 44*(1), 274–279. https://doi.org/10.1007/s10853-008-3045-8

Van Nong, H., Hung, L. X., Thang, P. N., Chinh, V. D., Vu, L. V., Dung, P. T., Trung, T. V., & Nga, P. T. (2016). Fabrication and vibration characterisation of curcumin extracted from turmeric (Curcuma longa) rhizomes of the northern Vietnam. SpringerPlus, 5, Article 1147. https://doi.org/10.1186/s40064-016-2812-2

Wei, H., Heidarshenas, B., Zhou, L., Hussain, G., Li, Q., & Ostrikov, K. (2020). Green inhibitors for steel corrosion in acidic environment: State of art. *Materials Today Sustainability, 10*, Article 100044. https://doi.org/10.1016/j.mtsust.2020.100044

Yıldız, R., Arslanhan, S., Döner, A., & Baran, M. F. (2024). Corrosion behaviour of mild steel in 1 M HCl with Cyclotrichium niveum as a green inhibitor. Materials Chemistry and Physics, 312, Article 128654. https://doi.org/10.1016/j.matchemphys.2023.128654

Zakeri, A., Bahmani, E., & Sabour Rouh Aghdam, A. (2022). Plant extracts as sustainable and green corrosion inhibitors for protection of ferrous metals in corrosive media: A mini review. *Corrosion Communications, 5*, 25–38. https://doi.org/10.1016/j.corcom.2022.03.002